

Numerical Investigations of Effects of Lorentz Force and Hydrodynamic Slip on the Flow Characteristics of an Upper-Convected Maxwell Viscoelastic Nanofluid in a Permeable Channel Embedded in a Porous Medium

M. G. Sobamowo^{1,*}, S. I. Alozie¹, A. A. Yinusa¹, A. O. Adedibu²,
M. O. Salami¹, S. O. Kehinde³

¹Department of Mechanical Engineering, University of Lagos, Akoka, Yaba, Lagos, Nigeria

²Department of Electrical and Electronics Engineering, the Polytechnic, Ibadan, Oyo, Nigeria

³Department of Mathematics, University of Lagos, Akoka, Yaba, Lagos, Nigeria

ABSTRACT

In this work, impacts of Lorentz force and hydrodynamic slip on the flow characteristics of an upper-convected Maxwell (UCM) nanofluid through a permeable microchannel embedded in porous medium are investigated numerically using fifth-order Runge–Kutta–Fehlberg method. Based on the parametric study, it is observed from the results that increase in slip parameter, nanoparticle concentration and Darcy number lead to increase in the velocity of the UCM fluid, while increase in Deborah's, Hartmann and Reynolds numbers decreases the fluid flow velocity towards the lower plate. But as the upper plate is approached, a reverse trend is observed. The study can be used to advance the application of UCM flow in the areas of biomedical, geophysical and astrophysics.

Keywords: Magnetic field, porous medium, slip analysis, upper-convected Maxwell flow, viscoelastic nanofluid

***Corresponding Author**

E-mail: mikegbeminiyiprof@yahoo.com

INTRODUCTION

The boundary layer flow of a viscoelastic fluid over a flat surface and channel has continued to find its various applications such as gaseous diffusion, blood flow through oxygenators and flow in blood capillaries which have continue to arouse the research interests. Also, there are various complex rheological fluids such as blood, paints, synovial fluid, saliva, jam which cannot be adequately described by Navier–Stokes equations. This leads to the development of complex constitutive relations to capture the flow behaviour of the

complex fluids [1]. Among the newly developed fluid models of the integral and differential-type models, upper-convected Maxwell (UCM) fluid model has showed to be an effective fluid model that captures these phenomena of fluids, especially of those with high elastic behaviours such as polymer melts since highly elastic fluids have high Deborah number [2, 3]. In the analysis of Maxwell flow, Fetecau [4] presented a new exact solution for flow through infinite microchannel, while Hunt [5] studied convective fluid flow through rectangular duct. Sheikholeslami et al. [6]

investigated magneto-hydrodynamic (MHD) field effect on flow through semi-porous channel utilizing analytical methods. Shortly after, Sheikholeslami [7–9] adopted numerical solutions in the investigations of nanofluid in semi-annulus enclosure. Flow of UCM fluid through porous stretch sheet was investigated by Raftari and Yildirim [10]. Entropy generation in fluid in the presence of magnetic field was analysed by Sheikholeslami and Ganji [11] using lattice Boltzmann method, while Ganji et al. [12] used analytical and numerical methods for the fluid-flow problems under the influence of magnetic field. The flow of viscoelastic fluid through a moving plate was analysed by Sadeghy and Sharifi [13] using local similarity solutions. Mass transfer and flow of chemically reactive UCM fluid under induced magnetic field was investigated by Vajrevulu et al. [14]. Not long after, Raftari and Vajrevulu [15] adopted the homotopy analysis method in the study of flow and heat transfer in stretching wall channels considering MHD. Hatami et al. [16] presented forced convective MHD nanofluid flow conveyed through horizontal parallel plates. Laminar thermal boundary flow layer over flat plate considering convective fluid surface was analysed by Aziz [17] using similarity solution. Beg and Makinde [18] examined the flow of viscoelastic fluid through Darcian microchannel with high permeability.

Most of the above review studies focused on the analysis of fluid flow under no-slip condition. However, such an assumption of no-slip condition does not hold in a flow system with small-size characteristics or low-flow pressure. The pioneer work of flow with slip boundary condition was first initiated by Navier [19]. Such an important condition (slip conditions) occurs in various flows such as nanofluids, polymeric liquids, fluids containing concentrated suspensions, flow on multiple interfaces,

thin-film problems and rarefied fluid problems [19–31]. Due to the practical implications of the condition of flow processes, several studies on the effects of slip boundary conditions on fluid-flow behaviours have been presented by many researchers [19–32]. Abbasi et al. [33] investigated the MHD flow characteristics of UCM viscoelastic flow in a permeable channel under slip conditions. However, to the best of the author's knowledge, a study on simultaneous effects of Lorentz force, slip, nanoparticle and porous medium on the flow characteristics of a UCM viscoelastic nanofluid has not been carried out in literature. Therefore, in this work, impacts of Lorentz force and hydrodynamic slip on the flow characteristics of a UCM nanofluid through a permeable microchannel embedded in porous medium are investigated. The nonlinear partial differential equations governing the flow phenomena are converted to a nonlinear ordinary differential equation using similarity transformation. Thereafter, the ordinary differential is solved numerically using fifth-order Runge–Kutta–Fehlberg method.

MODEL DEVELOPMENT AND ANALYTICAL SOLUTION

Consider a laminar slip flow of an electrically conducting fluid in a microchannel. Along the y -axis, magnetic fields are imposed uniformly, as described in the physical model diagram (Figure 1). It is assumed that external electric field is zero and electrical conductivity is constant. Therefore, magnetic Reynolds number is small and magnetic field induced by fluid motion is negligible.

Based on the assumptions, the governing equation for the Maxwell fluid is presented as [8] follows:

$$T - pI + S \quad (1)$$

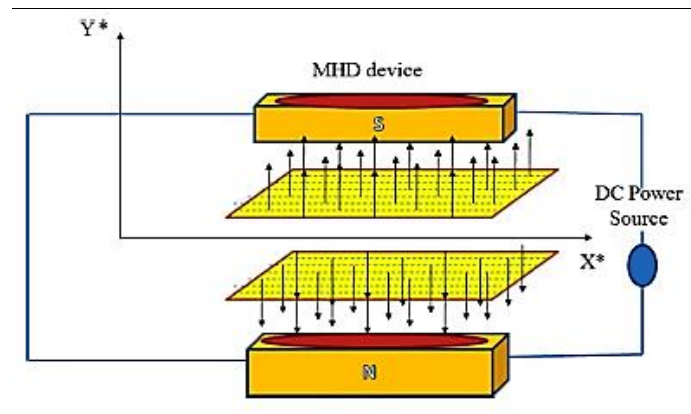


Fig. 1. Flow of upper-convected Maxwell fluid between permeable channels embedded in porous medium.

Where the Cauchy stress tensor is T and S is the extra-stress tensor which satisfies

$$S + \lambda \left(\frac{ds}{dt} - LS - SL^T \right) \mu A_L \quad (2)$$

The Rivlin–Ericksen tensor is defined by

$$A_L = \nabla V + (\nabla V)^T \quad (3)$$

The continuity and momentum equations for steady, incompressible, two-dimensional flows are expressed as

$$\frac{\partial \bar{u}}{\partial x} + \frac{\partial \bar{v}}{\partial y} = 0 \quad (4)$$

$$\rho_{nf} \left(u \frac{\partial u}{\partial x} + v \frac{\partial u}{\partial y} \right) = -\frac{\partial P}{\partial x} + \frac{\partial S_{xx}}{\partial x} + \frac{\partial S_{xy}}{\partial y} - \sigma_{nf} B^2(t) u - \frac{\mu_{nf} u}{K_p} \quad (5)$$

$$\rho_{nf} \left(\bar{u} \frac{\partial \bar{v}}{\partial x} + \bar{v} \frac{\partial \bar{v}}{\partial y} \right) = -\frac{\partial P}{\partial x} + \frac{\partial S_{yx}}{\partial x} + \frac{\partial S_{yy}}{\partial y} - \frac{\mu_{nf} \bar{v}}{K_p} \quad (6)$$

Where the effective density ρ_{nf} and effective dynamic viscosity μ_{nf} of the nanofluid are defined as follows:

$$\rho_{nf} = (1 - \phi) \rho_f + \phi \rho_s,$$

$$\mu_{nf} = \frac{\mu_f}{(1 - \phi)^{2.5}},$$

$$\sigma_{nf} = \sigma_f \left[1 + \frac{3 \left\{ \frac{\sigma_s}{\sigma_f} - 1 \right\} \phi}{\left\{ \frac{\sigma_s}{\sigma_f} + 2 \right\} \phi - \left\{ \frac{\sigma_s}{\sigma_f} - 1 \right\} \phi} \right],$$

And

S_{xx} , S_{xy} , S_{yx} and S_{yy} are extra-stress tensors and ρ is the density of the fluid. Using the shear-stress strain for a upper-convected liquid, the governing equations of fluid motion are easily expressed as [16]

$$\frac{\partial u}{\partial x} + \frac{\partial v}{\partial y} = 0 \quad (7)$$

$$u \frac{\partial u}{\partial x} + v \frac{\partial u}{\partial y} + \lambda \left(u^2 \frac{\partial^2 u}{\partial x^2} + v \frac{\partial^2 u}{\partial y^2} + 2uv \frac{\partial^2 u}{\partial x \partial y} \right) = v_{nf} \frac{\partial^2 u}{\partial y^2} - \frac{\sigma_{nf} B^2(t) u}{\rho_{nf}} - \frac{v_{nf} u}{K_p} \quad (8)$$

Where flow velocity component (u , v) are velocity component along the x - and y -directions, respectively. Since the flow is symmetric about channel centreline, attention is given to the flow region $0 < y < H$. Appropriate boundary condition is given as [14]

$$y = 0: \frac{\partial u}{\partial x} = 0, v = 0 \quad (9)$$

$$y = H: \frac{\partial u}{\partial y} = -\beta u, v = V_w \quad (10)$$

where V_w and β are the wall characteristic suction velocity and sliding friction, respectively.

The physical and thermal properties of the base fluid and nanoparticles are given in Tables 1 and Table 2, respectively.

Table 1: Physical and thermal properties of the base fluid

Base Fluid	ρ (kg/m ³)	C_p (J/kg K)	k (W/m K)	$\sigma(\Omega^{-1}\text{m}^{-1})$
Pure water	997.1	4179	0.613	5.50
Ethylene glycol	1115	2430	0.253	1.07
Engine oil	884	1910	0.144	4.02
Kerosene	783	2010	0.145	4.01

Table 2: Physical and thermal properties of nanoparticles

Nanoparticles	ρ (kg/m ³)	C_p (J/kg K)	k (W/m K)	$\sigma(\Omega^{-1}\text{m}^{-1})$
Copper (Cu)	8933	385	401	59.6
Aluminium oxide (Al ₂ O ₃)	3970	765	40	16.7
SWCNTs	2600	42.5	6600	0.429
Silver (Ag)	10500	235.0	429	
Titanium dioxide (TiO ₂)	4250	686.2	8.9538	
Copper (II) oxide (CuO)	783	540	18	

The similarity variables are introduced as follows:

$$\eta = \frac{y}{H}, \quad u = -V_w x f'(y); \quad v = V_w f(y); \quad k = \frac{\mu}{H\beta} \tag{11}$$

With the aid of the dimensionless parameters in Equation (11), the constitutive relation is satisfied. Equations (2)–(4) can be expressed as follows:

$$f''' - \left(M^2 + \frac{1}{Da}\right) f' + (1-\phi)^{2.5} \left((1-\phi) + \phi \frac{\rho_s}{\rho_f} \right) Re_w (f'^2 - ff'') + De(1-\phi)^{2.5} (2ff'f'' - f^2f''') = 0 \tag{12}$$

And the boundary conditions as

$$\begin{aligned} \eta = 0 : f'' = 0; f = 0 \\ \eta = 1 : f' = -kf'' : f = 1 \end{aligned} \tag{13}$$

Where $Re_w = \frac{V_w H}{\nu}$ is the Reynolds number, $De = \frac{\lambda V_w^2}{\nu}$ is the Deborah’s number, $M^2 = \frac{\sigma B_0^2 H}{\mu}$ is the Hartman parameter, $Da = \frac{K_p}{H}$ is the Darcy’s number. For $Re_w > 0$ corresponds to suction flow, while $Re_w < 0$ corresponds to injection flow, respectively.

Equation (13) is a third-order differential equation with four boundary conditions, through a creative differentiation of Equation (12). Hence introducing fourth-order equation as

$$f^{iv} - \left(M^2 + \frac{1}{Da}\right) f'' + (1-\phi)^{2.5} \left((1-\phi) + \phi \frac{\rho_s}{\rho_f} \right) Re_w (ff'' - ff''') + De(1-\phi)^{2.5} (2f'^2 f'' - 2ff''^2 + f^2 f^{iv}) = 0 \tag{14}$$

Equation (14) satisfies all the four boundary conditions in Equation (13).

NUMERICAL PROCEDURE FOR THE ANALYSIS OF THE GOVERNING EQUATION

Equation (14) is a fourth-order ordinary differential equation which is, in this work, analysed numerically using fifth-order Runge–Kutta–Fehlberg method (Cash–Karp Runge–Kutta) coupled with shooting method. Since Runge–Kutta method is for solving first-order ordinary

differential equation, the fourth-order ordinary differential equation is decomposed into a system of first-order differential equations as follows:

$$f' = p, \quad (15a)$$

$$f'' = p' = q, \quad (15b)$$

$$f''' = q' = z, \quad (15c)$$

$$z' - \left(M^2 + \frac{1}{Da} \right) q + (1-\phi)^{2.5} \left((1-\phi) + \phi \frac{\rho_s}{\rho_f} \right) Re_w (pq - fq) + De(1-\phi)^{2.5} (2p^2q - 2fq^2 + f^2z') = 0 \quad (15d)$$

Equations (15a)–(15b) can be written as follows:

$$a(\eta, f, p, q, z) = p, \quad (16a)$$

$$b(\eta, f, p, q, z) = q, \quad (16b)$$

$$c(\eta, f, p, q, z) = z, \quad (16c)$$

$$d(\eta, f, p, q, z) = \frac{\left(M^2 + \frac{1}{Da} \right) q - (1-\phi)^{2.5} \left((1-\phi) + \phi \frac{\rho_s}{\rho_f} \right) Re_w (pq - fq) - De(1-\phi)^{2.5} (2p^2q - 2fq^2)}{(1 + De(1-\phi)^{2.5} f^2)} \quad (16d)$$

The iterative scheme of the fifth-order Runge–Kutta–Fehlberg method (Cash–Karp Runge–Kutta) for the above system of first-order equations is given as follows:

$$f_{i+1} = f_i + h \left(\frac{2835}{27648} k_1 + \frac{18575}{48384} k_3 + \frac{13525}{55296} k_4 + \frac{277}{14336} k_5 + \frac{1}{4} k_6 \right)$$

$$p_{i+1} = p_i + h \left(\frac{2835}{27648} l_1 + \frac{18575}{48384} l_3 + \frac{13525}{55296} l_4 + \frac{277}{14336} l_5 + \frac{1}{4} l_6 \right)$$

$$q_{i+1} = q_i + h \left(\frac{2835}{27648} m_1 + \frac{18575}{48384} m_3 + \frac{13525}{55296} m_4 + \frac{277}{14336} m_5 + \frac{1}{4} m_6 \right)$$

$$z_{i+1} = z_i + h \left(\frac{2835}{27648} r_1 + \frac{18575}{48384} r_3 + \frac{13525}{55296} r_4 + \frac{277}{14336} r_5 + \frac{1}{4} r_6 \right)$$

where

$$k_1 = a(\eta_i, f_i, p_i, q_i, z_i)$$

$$l_1 = b(\eta_i, f_i, p_i, q_i, z_i)$$

$$m_1 = c(\eta_i, f_i, p_i, q_i, z_i)$$

$$r_1 = d(\eta_i, f_i, p_i, q_i, z_i)$$

$$\begin{aligned}
 k_2 &= a \left(\eta_i + \frac{1}{5}h, f_i + \frac{1}{5}k_1h, p_i + \frac{1}{5}l_1h, q_i + \frac{1}{5}m_1h, z_i + \frac{1}{5}r_1h \right) \\
 l_2 &= b \left(\eta_i + \frac{1}{5}h, f_i + \frac{1}{5}k_1h, p_i + \frac{1}{5}l_1h, q_i + \frac{1}{5}m_1h, z_i + \frac{1}{5}r_1h \right) \\
 m_2 &= c \left(\eta_i + \frac{1}{5}h, f_i + \frac{1}{5}k_1h, p_i + \frac{1}{5}l_1h, q_i + \frac{1}{5}m_1h, z_i + \frac{1}{5}r_1h \right) \\
 r_2 &= d \left(\eta_i + \frac{1}{5}h, f_i + \frac{1}{5}k_1h, p_i + \frac{1}{5}l_1h, q_i + \frac{1}{5}m_1h, z_i + \frac{1}{5}r_1h \right) \\
 k_3 &= a \left(\eta_i + \frac{3}{10}h, f_i + \frac{3}{40}k_1h + \frac{9}{40}k_2h, p_i + \frac{3}{40}l_1h + \frac{9}{40}l_2h, \right. \\
 &\quad \left. q_i + \frac{3}{40}m_1h + \frac{9}{40}m_2h, z_i + \frac{3}{40}r_1h + \frac{9}{40}r_2h \right) \\
 l_3 &= b \left(\eta_i + \frac{3}{10}h, f_i + \frac{3}{40}k_1h + \frac{9}{40}k_2h, p_i + \frac{3}{40}l_1h + \frac{9}{40}l_2h, \right. \\
 &\quad \left. q_i + \frac{3}{40}m_1h + \frac{9}{40}m_2h, z_i + \frac{3}{40}r_1h + \frac{9}{40}r_2h \right) \\
 m_3 &= c \left(\eta_i + \frac{3}{10}h, f_i + \frac{3}{40}k_1h + \frac{9}{40}k_2h, p_i + \frac{3}{40}l_1h + \frac{9}{40}l_2h, \right. \\
 &\quad \left. q_i + \frac{3}{40}m_1h + \frac{9}{40}m_2h, z_i + \frac{3}{40}r_1h + \frac{9}{40}r_2h \right) \\
 r_3 &= d \left(\eta_i + \frac{3}{10}h, f_i + \frac{3}{40}k_1h + \frac{9}{40}k_2h, p_i + \frac{3}{40}l_1h + \frac{9}{40}l_2h, \right. \\
 &\quad \left. q_i + \frac{3}{40}m_1h + \frac{9}{40}m_2h, z_i + \frac{3}{40}r_1h + \frac{9}{40}r_2h \right) \\
 k_4 &= a \left(\eta_i + \frac{3}{5}h, f_i + \frac{3}{10}k_1h - \frac{9}{10}k_2h + \frac{6}{5}k_3h, p_i + \frac{3}{10}l_1h - \frac{9}{10}l_2h + \frac{6}{5}l_3h, \right. \\
 &\quad \left. q_i + \frac{3}{10}m_1h - \frac{9}{10}m_2h + \frac{6}{5}m_3h, z_i + \frac{3}{10}r_1h - \frac{9}{10}r_2h + \frac{6}{5}r_3h \right) \\
 l_4 &= b \left(\eta_i + \frac{3}{5}h, f_i + \frac{3}{10}k_1h - \frac{9}{10}k_2h + \frac{6}{5}k_3h, p_i + \frac{3}{10}l_1h - \frac{9}{10}l_2h + \frac{6}{5}l_3h, \right. \\
 &\quad \left. q_i + \frac{3}{10}m_1h - \frac{9}{10}m_2h + \frac{6}{5}m_3h, z_i + \frac{3}{10}r_1h - \frac{9}{10}r_2h + \frac{6}{5}r_3h \right) \\
 m_4 &= c \left(\eta_i + \frac{3}{5}h, f_i + \frac{3}{10}k_1h - \frac{9}{10}k_2h + \frac{6}{5}k_3h, p_i + \frac{3}{10}l_1h - \frac{9}{10}l_2h + \frac{6}{5}l_3h, \right. \\
 &\quad \left. q_i + \frac{3}{10}m_1h - \frac{9}{10}m_2h + \frac{6}{5}m_3h, z_i + \frac{3}{10}r_1h - \frac{9}{10}r_2h + \frac{6}{5}r_3h \right) \\
 r_4 &= d \left(\eta_i + \frac{3}{5}h, f_i + \frac{3}{10}k_1h - \frac{9}{10}k_2h + \frac{6}{5}k_3h, p_i + \frac{3}{10}l_1h - \frac{9}{10}l_2h + \frac{6}{5}l_3h, \right. \\
 &\quad \left. q_i + \frac{3}{10}m_1h - \frac{9}{10}m_2h + \frac{6}{5}m_3h, z_i + \frac{3}{10}r_1h - \frac{9}{10}r_2h + \frac{6}{5}r_3h \right)
 \end{aligned}$$

$$\begin{aligned}
k_5 &= a \left(\begin{array}{l} \eta_i + h, f_i - \frac{11}{54}k_1h + \frac{5}{2}k_2h - \frac{70}{27}k_3h + \frac{35}{27}k_4h, p_i - \frac{11}{54}l_1h + \frac{5}{2}l_2h - \frac{70}{27}l_3h + \frac{35}{27}l_4h, \\ q_i - \frac{11}{54}m_1h + \frac{5}{2}m_2h - \frac{70}{27}m_3h + \frac{35}{27}m_4h, z_i - \frac{11}{54}r_1h + \frac{5}{2}r_2h - \frac{70}{27}r_3h + \frac{35}{27}r_4h \end{array} \right) \\
l_5 &= b \left(\begin{array}{l} \eta_i + h, f_i - \frac{11}{54}k_1h + \frac{5}{2}k_2h - \frac{70}{27}k_3h + \frac{35}{27}k_4h, p_i - \frac{11}{54}l_1h + \frac{5}{2}l_2h - \frac{70}{27}l_3h + \frac{35}{27}l_4h, \\ q_i - \frac{11}{54}m_1h + \frac{5}{2}m_2h - \frac{70}{27}m_3h + \frac{35}{27}m_4h, z_i - \frac{11}{54}r_1h + \frac{5}{2}r_2h - \frac{70}{27}r_3h + \frac{35}{27}r_4h \end{array} \right) \\
m_5 &= c \left(\begin{array}{l} \eta_i + h, f_i - \frac{11}{54}k_1h + \frac{5}{2}k_2h - \frac{70}{27}k_3h + \frac{35}{27}k_4h, p_i - \frac{11}{54}l_1h + \frac{5}{2}l_2h - \frac{70}{27}l_3h + \frac{35}{27}l_4h, \\ q_i - \frac{11}{54}m_1h + \frac{5}{2}m_2h - \frac{70}{27}m_3h + \frac{35}{27}m_4h, z_i - \frac{11}{54}r_1h + \frac{5}{2}r_2h - \frac{70}{27}r_3h + \frac{35}{27}r_4h \end{array} \right) \\
r_5 &= d \left(\begin{array}{l} \eta_i + h, f_i - \frac{11}{54}k_1h + \frac{5}{2}k_2h - \frac{70}{27}k_3h + \frac{35}{27}k_4h, p_i - \frac{11}{54}l_1h + \frac{5}{2}l_2h - \frac{70}{27}l_3h + \frac{35}{27}l_4h, \\ q_i - \frac{11}{54}m_1h + \frac{5}{2}m_2h - \frac{70}{27}m_3h + \frac{35}{27}m_4h, z_i - \frac{11}{54}r_1h + \frac{5}{2}r_2h - \frac{70}{27}r_3h + \frac{35}{27}r_4h \end{array} \right) \\
k_6 &= a \left(\begin{array}{l} \eta_i + \frac{7}{8}h, f_i + \frac{1631}{55296}k_1h + \frac{175}{512}k_2h + \frac{575}{13824}k_3h + \frac{44275}{110592}k_4h + \frac{253}{4096}k_5h, \\ p_i + \frac{1631}{55296}l_1h + \frac{175}{512}l_2h + \frac{575}{13824}l_3h + \frac{44275}{110592}l_4h + \frac{253}{4096}l_5h, \\ q_i + \frac{1631}{55296}m_1h + \frac{175}{512}m_2h + \frac{575}{13824}m_3h + \frac{44275}{110592}m_4h + \frac{253}{4096}m_5h, \\ z_i + \frac{1631}{55296}r_1h + \frac{175}{512}r_2h + \frac{575}{13824}r_3h + \frac{44275}{110592}r_4h + \frac{253}{4096}r_5h \end{array} \right) \\
l_6 &= b \left(\begin{array}{l} \eta_i + \frac{7}{8}h, f_i + \frac{1631}{55296}k_1h + \frac{175}{512}k_2h + \frac{575}{13824}k_3h + \frac{44275}{110592}k_4h + \frac{253}{4096}k_5h, \\ p_i + \frac{1631}{55296}l_1h + \frac{175}{512}l_2h + \frac{575}{13824}l_3h + \frac{44275}{110592}l_4h + \frac{253}{4096}l_5h, \\ q_i + \frac{1631}{55296}m_1h + \frac{175}{512}m_2h + \frac{575}{13824}m_3h + \frac{44275}{110592}m_4h + \frac{253}{4096}m_5h, \\ z_i + \frac{1631}{55296}r_1h + \frac{175}{512}r_2h + \frac{575}{13824}r_3h + \frac{44275}{110592}r_4h + \frac{253}{4096}r_5h \end{array} \right) \\
m_6 &= c \left(\begin{array}{l} \eta_i + \frac{7}{8}h, f_i + \frac{1631}{55296}k_1h + \frac{175}{512}k_2h + \frac{575}{13824}k_3h + \frac{44275}{110592}k_4h + \frac{253}{4096}k_5h, \\ p_i + \frac{1631}{55296}l_1h + \frac{175}{512}l_2h + \frac{575}{13824}l_3h + \frac{44275}{110592}l_4h + \frac{253}{4096}l_5h, \\ q_i + \frac{1631}{55296}m_1h + \frac{175}{512}m_2h + \frac{575}{13824}m_3h + \frac{44275}{110592}m_4h + \frac{253}{4096}m_5h, \\ z_i + \frac{1631}{55296}r_1h + \frac{175}{512}r_2h + \frac{575}{13824}r_3h + \frac{44275}{110592}r_4h + \frac{253}{4096}r_5h \end{array} \right)
\end{aligned}$$

$$r_6 = d \left(\begin{array}{l} \eta_i + \frac{7}{8}h, f_i + \frac{1631}{55296}k_1h + \frac{175}{512}k_2h + \frac{575}{13824}k_3h + \frac{44275}{110592}k_4h + \frac{253}{4096}k_5h, \\ p_i + \frac{1631}{55296}l_1h + \frac{175}{512}l_2h + \frac{575}{13824}l_3h + \frac{44275}{110592}l_4h + \frac{253}{4096}l_5h, \\ q_i + \frac{1631}{55296}m_1h + \frac{175}{512}m_2h + \frac{575}{13824}m_3h + \frac{44275}{110592}m_4h + \frac{253}{4096}m_5h, \\ z_i + \frac{1631}{55296}r_1h + \frac{175}{512}r_2h + \frac{575}{13824}r_3h + \frac{44275}{110592}r_4h + \frac{253}{4096}r_5h \end{array} \right)$$

Using the above fifth-order Runge–Kutta–Fehlberg method coupled with shooting method, computer programs are written in MATLAB for the solutions of Equation (14). The results for step size, $h = 0.01$, are presented in the following section.

RESULTS AND DISCUSSION

Using copper nanoparticle and water, the results obtained from the analytical solution are shown graphically in Figures 2–9, when $Re_w=8, De=0.1, M=2, \hbar = 0.1, Da=2$ and $\phi = 0.01$, unless otherwise stated. Figures illustrate the influence of nanoparticle concentration (ϕ) on the flow process. As shown from the figures, the quantitative increase of the nanoparticle concentration causes increase in the velocity distribution. It is very important to indicate viscoelastic nature of the fluid. Therefore, the effects of Deborah’s number on the flow process are depicted in Figure 3. It is illustrated that increase in Deborah’s number (De) illustrates the UCM as highly elastic fluid (such as polymeric melts) that depicts decrease in fluid-flow velocity.

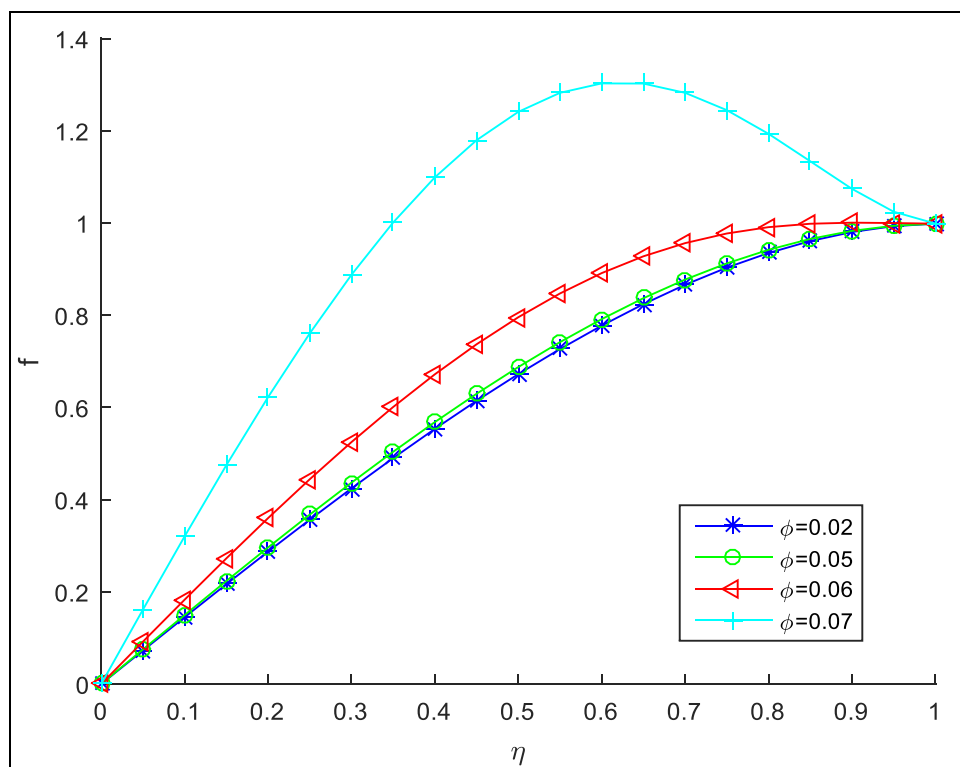


Fig. 2. Effect of nanoparticle concentration number (ϕ) on the axial velocity of the flow process.

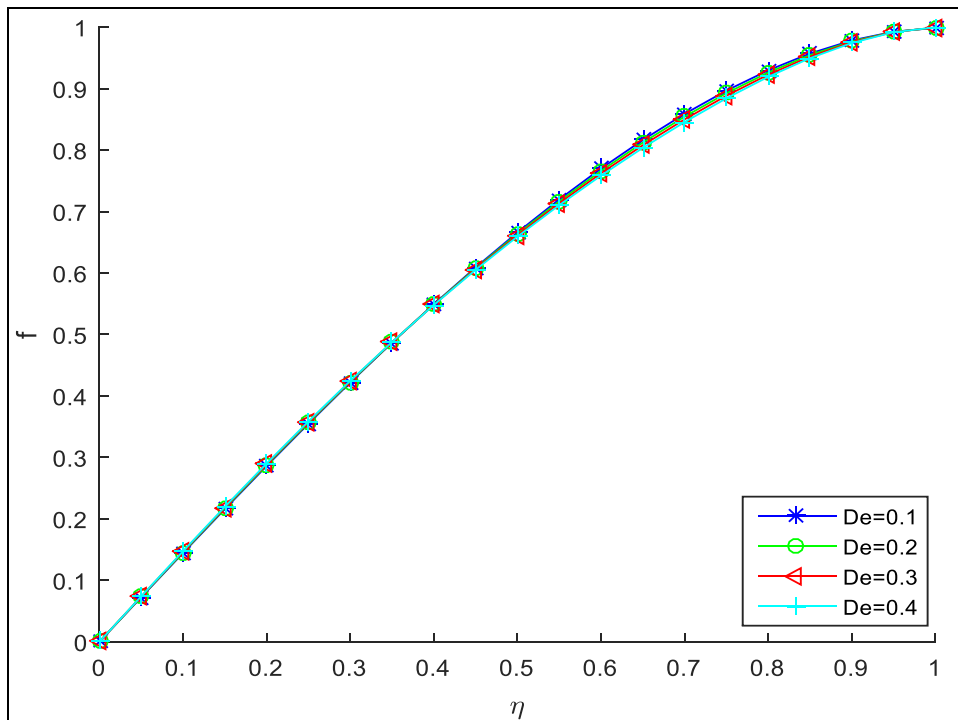


Fig. 3. Effect of Deborah's number (De) on the axial velocity of the flow process.

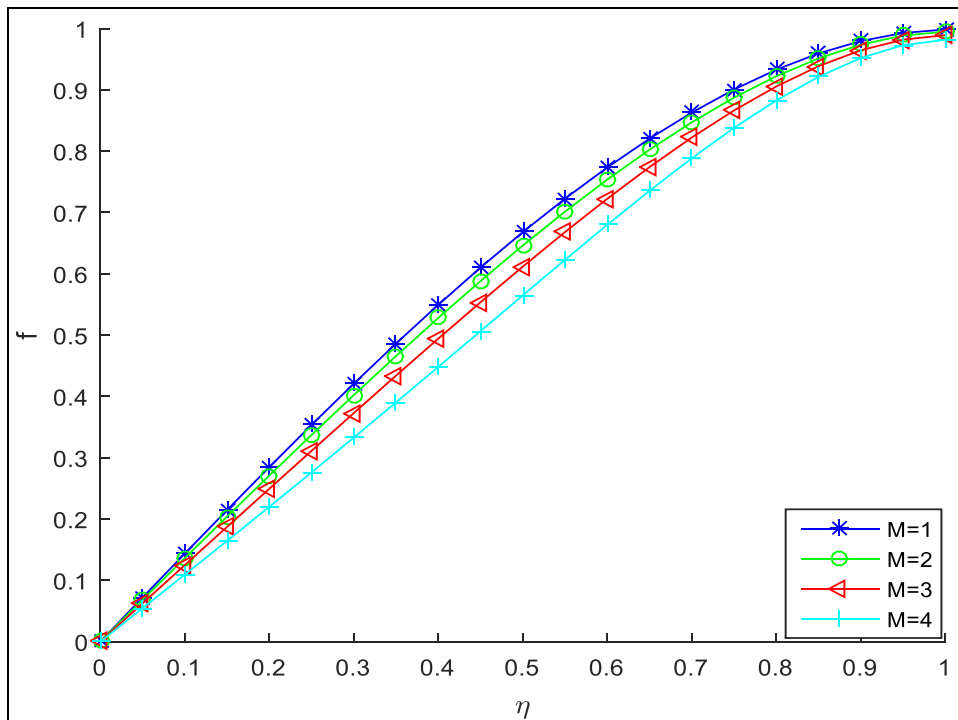


Fig. 4. Effect of Hartmann parameter (M) on the axial velocity of the flow process.

The influence of magnetic field parameter on flow of the UCM fluid under is depicted in Figure 4. As observed in the figure, the numerical increase of the magnetic or Hartmann parameter (M) shows

decreasing velocity profile. This is because the applied magnetic field produces a damping effect (Lorentz force) on the flow process. This damping effect increases as the quantitative or numerical

value of the Hartmann number increases. It should be noted that the effect of magnetic field parameter is maximum towards the upper flow channel. In order to show the effect of the permeability of the

porous medium on the flow, effect of Darcy parameter (Da) on fluid transport is illustrated in Figure 5. Increasing Darcy number demonstrates increasing velocity profile as shown in the figure.

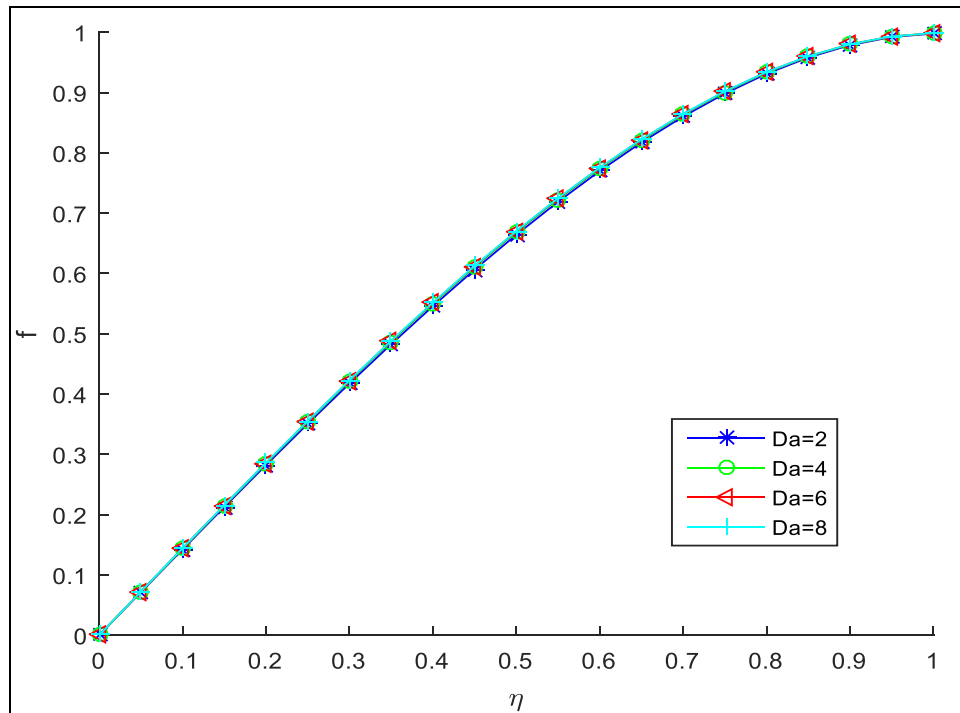


Fig. 5. Effect of Darcy's number (Da) on the axial velocity of the flow process.

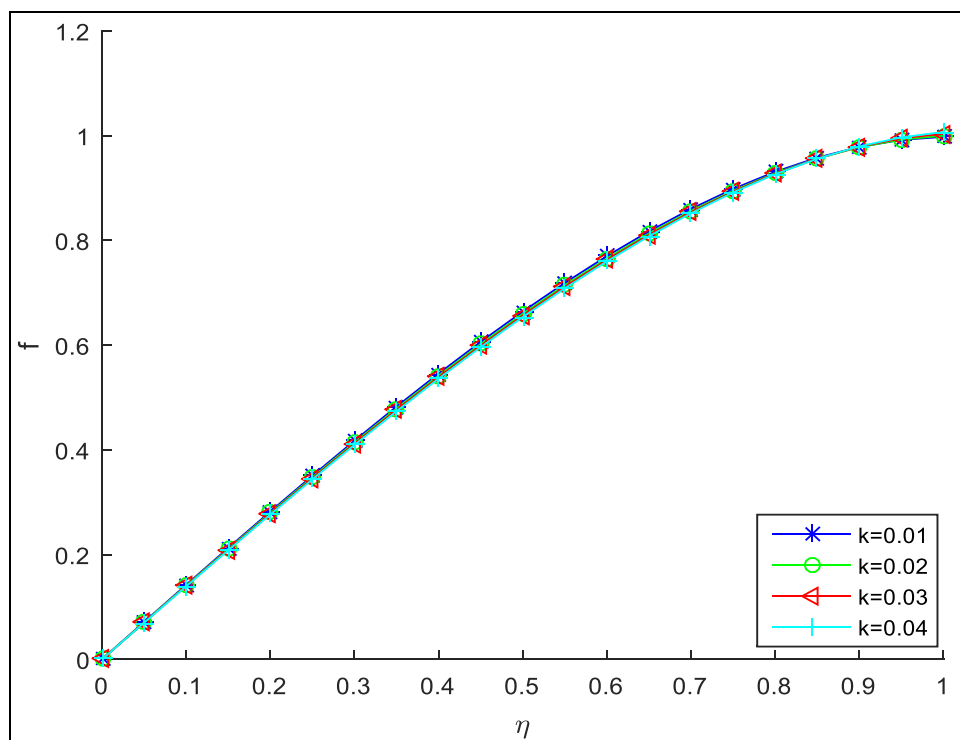


Fig. 6. Effect of slip parameter (k) on the axial velocity of the flow process.

Figure 6 shows the effect of fluid slip parameter (k) on the velocity of the fluid flow. It should be noted that the slip parameter depicts that the fluid velocity at the boundary is not at equal velocity with fluid particles closest to flow boundary due to large variance in macro- and micro-fluid

flow. As observed from Figure 6, increasing the slip parameter leads to decreasing velocity distributions of the process. In order to show the relative significance of the inertia effect as compared to the viscous effect, the effect of Reynolds number on the flow phenomena is illustrated in Figure 7.

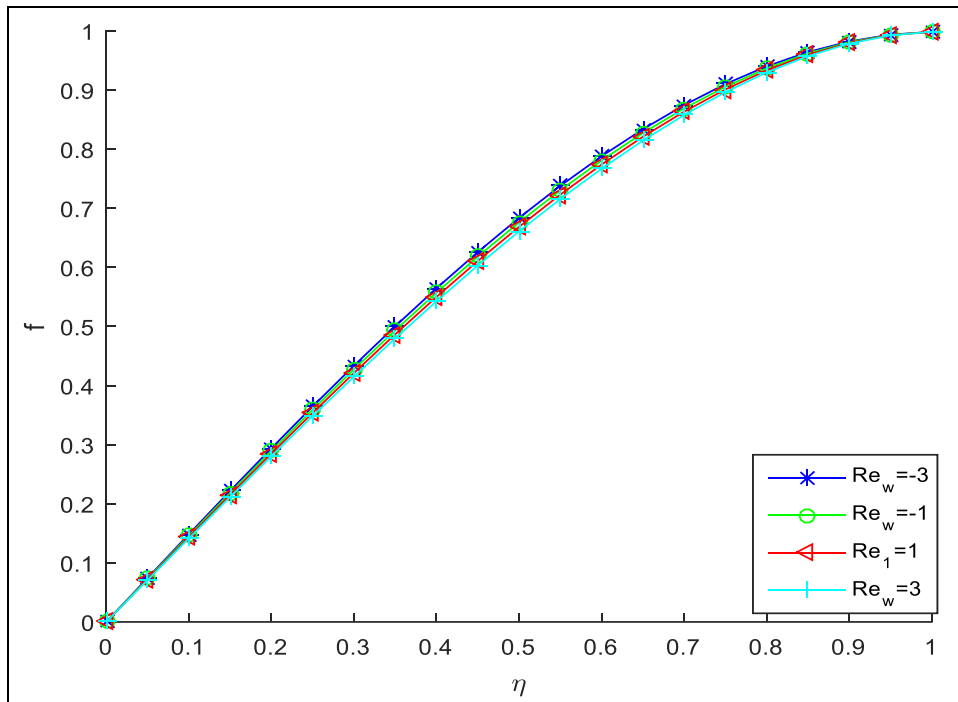


Fig. 7. Effect of Reynolds number (Re_w) on the axial velocity of the flow process.

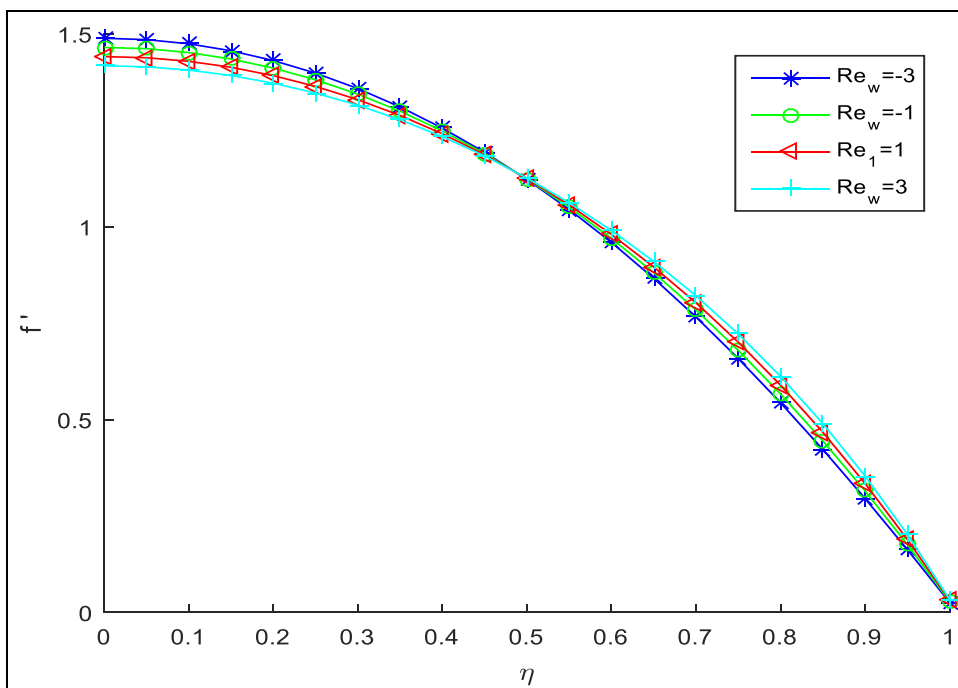


Fig. 8. Effect of Reynolds number (Re_w) on the radial velocity of the flow process.

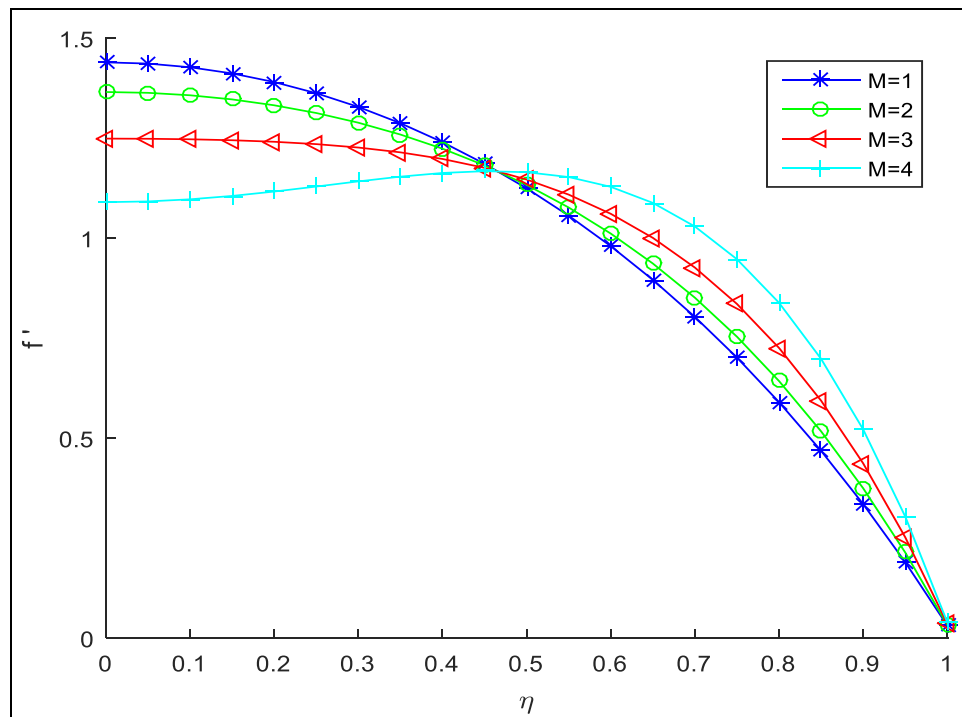


Fig. 9. Effect of Hartman parameter (M) on the radial velocity of the flow process.

It is established from the graphical display that increasing Reynolds number (Re_w) causes decrease in flow profile whose effect is maximum towards the upper plate.

Figure 8 shows the effect of increasing Reynolds number on the radial velocity component of the flow. It is shown that increasing the Reynolds number causes decrease in velocity distribution but as flow reaches the mid-plate around $\eta = 0.5$ (not determined accurately), an increasing velocity distribution is seen. However, effect is minimal towards the upper plate. Also, influence of magnetic field on radial velocity is depicted in Figure 9, as a significant increase in velocity is seen due to quantitative increase of Hartmann parameter (M) towards the lower plate, while as upper plate is approached, a reverse trend is observed.

CONCLUSION

In this work, impacts of Lorentz force and hydrodynamic slip on the flow characteristics of an UCM nanofluid through a permeable microchannel

embedded in porous medium have been investigated numerically using fifth-order Runge–Kutta–Fehlberg method. Important fluid parameter effects such as Deborah’s number, Darcy parameter and Hartman parameter were investigated on flow that increases in slip parameter, nanoparticle concentration and Darcy number which lead to increase in the velocity of the UCM fluid, while increase in Deborah’s, Hartmann, and Reynolds numbers decrease the fluid-flow velocity towards the lower plate. But as the upper plate is approached, a reverse trend is observed. The results obtained in this work may be used to further UCM fluid in applications in biomedical, astrophysics, geosciences, etc.

NOMENCLATURE

- Re_w Reynolds number
- M Hartman parameter
- k Slip parameter
- De Deborah’s number
- h Auxiliary parameter
- v^* y axis velocity component
- u^* x axis velocity component
- x Dimensionless horizontal coordinate

y Dimensionless vertical coordinate
 x^* Distance in x axis parallel to plate
 y^* Distance in y axis parallel to plate
 Da Darcy number

Greek Symbols

ρ Fluid density
 λ Relaxation time
 ν Kinematic viscosity
 β Sliding friction
 ϕ Nanoparticle concentration

REFERENCES

- [1] Bird RB, Armstrong RC, Hassager O. *Dynamics of Polymeric Liquids*, Vols. I and II. New York: Wiley; 1987.
- [2] Sadeghy K, Najafi AH, Saffaripour M. Sakiadis flow of an upper-convected Maxwell fluid. *Int J Nonlinear Mech.* 2005; 40: 1220–1228p.
- [3] Ziabaksh Z, Domairry G. Solution of laminar viscous flow in semi porous channel in the presence of a uniform magnetic field by using homotopy analysis method. *Commun Nonlinear Sci Numer Simul.* 2009; 14(4): 1284–1294p.
- [4] Fetecau C. A new exact solution for the flow of a Maxwell fluid past an infinite plate. *Int J Nonlinear Mech.* 2003; 38: 423–427p.
- [5] Hunt JCR. Magnetohydrodynamic flow in rectangular ducts. *J Fluid Mech.* 1965; 21: 577–590p.
- [6] Sheikholeslami M, Hatami M, Ganji DD. Analytical investigation of MHD nanofluid flow in a semi-porous channel. *Powder Technol.* 2013; 246: 327–336p.
- [7] Sheikholeslami M, Gorji-Bandpy M, Ganji DD. Numerical investigation of MHD effects on Al_2O_3 -water nanofluid flow and heat transfer in a semi-annulus using LBM. *Energy.* 2013; 60: 501–510p.
- [8] Sheikholeslami M, Gorji-Bandpy M, Ganji DD. Lattice Boltzman method for MHD natural convection heat transfer using nanofluid. *Powder Technol.* 2014; 254: 82–93p.
- [9] Sheikholeslami M, Hatami M, Ganji DD. Nanofluid flow and heat transfer in a rotating system in the presence of a magnetic field. *J Molec Liq.* 2014; 190: 112–120p.
- [10] Raftari B, Yildirim A. The application of homotopy perturbation method for MHD flows above porous stretching sheets. *Comput Appl Mech.* 2010; 59: 740–744p.
- [11] Sheikholeslami M, Ganji DD. Entropy generation of nanofluid in presence of magnetic field using lattice boltzmann method. *Phys A.* 2015; 417: 273–286p.
- [12] Ganji DD, Kachapi H, Seyed H. Analytical and numerical method in engineering and applied science. *Progr Nonlinear Sci.* 2011; 3: 570–579p.
- [13] Sadeghy K, Sharifi M. Local similarity solution for the flow of a “second grade” viscoelastic fluid above a moving plate. *Int J Nonlinear Mech.* 2004; 39: 1265–1273p.
- [14] Vajrevulu K, Prasad KV, Sujatha A. MHD flow and mass transfer of chemically reactive upper convected Maxwell fluid past porous surface. *Appl Math Mech.* 2012; 33(7): 899–910p.
- [15] Raftari B, Vajrevulu K. Homotopy analysis method for MHD viscoelastic fluid flow and heat transfer in a channel with a stretching wall. *Commun Nonlinear Sci Simul.* 2012; 17(11): 4149–4162p.
- [16] Hatami M, Nouri R, Ganji DD. Forced convection analysis for MHD Al_2O_3 -water nanofluid flow over a horizontal plate. *J Molec Liq.* 2013; 187: 294–301p.
- [17] Aziz A. A similarity solution for laminar thermal boundary layer over a flat plat with a convective surface boundary condition. *Commun Nonlinear Sci Numer Simul.* 2009; 14: 1064–1068p.

- [18] Beg OA, Makinde OD. Viscoelastic flow and species transfer in a Darcian high permeability channel. *J Petrol Sci Eng.* 2011; 76: 93–99p.
- [19] Navier CLMH. Memoir sur les lois du mouvement des fluids. *Mem Acad R Sci Inst France.* 1823; 6: 389–440p.
- [20] Choi CH, Westin JA, Breur KS. To slip or not slip water flows in hydrophilic and hydrophobic microchannels. *Proceedings of IMECE 2002.* New Orleans, LA. 2002. Article ID: 33707.
- [21] Matthew MT, Boyd ID. Nano boundary layer equation with nonlinear Navier boundary condition. *J Math Anal Appl.* 2007; 333: 381–400p.
- [22] Martin MJ, Boyd LD. Momentum and heat transfer in a laminar boundary layer with slip flow. *J Thermophys Heat Transf.* 2006; 20(4): 710–719p.
- [23] Ariel PD. Axisymmetric flow due to stretching sheet with partial slip. *Comput Math Appl.* 2007; 333: 381–400p.
- [24] Wang C. Analysis of viscous flow due to a stretching sheet with surface slip and suction. *Nonlinear Anal Real World Appl.* 2009; 10(1): 375–380p.
- [25] Das K. Impact of thermal radiation on MHD slip flow over a flat plate with variable fluid properties. *Heat Mass Transf.* 2012; 48: 767–778p.
- [26] Das K. Slip effects on heat and mass transfer in MHD micro polar fluid flow over an inclined plate with thermal radiation and chemical reaction. *Int J Numer Meth Fluids.* 2016; 70: 96–101p.
- [27] Hussain A, Mohyud-Din ST, Cheema TA. Analytical and numerical approaches to squeezing flow and heat transfer between two parallel disks with velocity slip and temperature jump. *China Phys Lett.* 2012; 29: 1–5p.
- [28] Das K. Slip flow and convective heat transfer of nanofluid over a permeable stretching surface. *Comput Phys.* 2012; 64(1): 34–42p.
- [29] Deissler RG. An analysis of second-order slip flow and temperature-jump boundary conditions for rarefied gases. *Int J Heat Mass Transf.* 1964; 7(6): 681–694p.
- [30] Das K, Jana S, Acharya N. Slip effects on squeezing flow of nanofluid between two parallel disks. *Int J Appl Mech Eng.* 2016; 21(1): 5–20p.
- [31] Ellahi R, Hayat T, Mahomed FM, Asghar S. Effects of slip on nonlinear flows of a third grade fluid. *Nonlinear Anal Real World Appl.* 2010; 11: 139–146p.
- [32] Malvadi A, Hedayati F, Ganji DD. Slip effects on unsteady stagnation point flow of a nanofluid over a stretching sheet. *Powd Technol.* 2014; 253: 377–384p.
- [33] Abbasi M, Khaki M, Rahbari A, Ganji DD. Analysis of MHD flow characteristics of an UCM viscoelastic flow in a permeable channel under slip conditions. *J Braz Soc Mech Eng Sci.* DOI 10.1007/s40430-015-0325-5, 2015.

Cite this Article: M. G. Sobamowo, S. I. Alozie, A. A. Yinusa, A. O. Adedibu, M. O. Salami, S. O. Kehinde. Numerical Investigations of Effects of Lorentz Force and Hydrodynamic Slip on the Flow Characteristics of an Upper-Convected Maxwell Viscoelastic Nanofluid in a Permeable Channel Embedded in a Porous Medium. *International Journal of Thermal Energy and Applications.* 2019; 1(2): 28–41p.